




Ginsenoside Rb1 Deters Cell Proliferation, Induces Apoptosis, Alleviates Oxidative Stress, and Antimetastasis in Oral Squamous Carcinoma Cells

Le An¹ · Yang Yu² · Long He¹ · Xu Xiao¹ · Pengcheng Li¹ 

Accepted: 12 February 2024

© The Author(s), under exclusive licence to Springer Science+Business Media, LLC, part of Springer Nature 2024

Abstract

There are numerous therapeutic applications for ginsenoside Rb1 (GRb1), the primary saponin derived from ginseng root. According to earlier research, ginsenoside Rb1 causes apoptosis and reduces the cell cycle. Its adverse effects, especially those on the development of the embryo, still need to be thoroughly studied. A host's lifestyle choices, including smoking, drinking too much alcohol, using tobacco products, and having an HPV infection, can increase the risk of oral squamous cell carcinoma (OSCC), one of the most prevalent malignancies of the oral cavity. To address this challenge, this investigation focuses on the design of GRb1 for treating OSCC. In vitro cytotoxicity studies confirmed that GRb1 was more effective in PCI-9A and PCI-13 cells, with reduced toxicity in non-cancerous cells. Further verification of cellular morphology was achieved through various biochemical staining methods. The mechanism of cell death was investigated by Annexin V-FITC and PI methods. Additionally, the antimetastatic attributes of GRb1 have been evaluated using both migration scratch and Transwell migration assays, which have collectively revealed excellent antimetastatic potential. The DNA fragmentation of the PCI-9A and PCI-13 cells was assessed using a comet assay. Ginsenoside Rb1 improved ROS levels and caused mitochondrial membrane potential alterations and DNA damage, which resulted in apoptosis. OSCC administration significantly reduced the levels of SOD, GSH, GPx, and CAT, increasing the levels of PCI-9A and PCI-13 cells, while GRb1 improved this situation. Therefore, we propose that Ginsenoside Rb1 could be an alternative therapeutic strategy for OSCC therapy.

Keywords Ginsenoside Rb1 · Oral squamous · Apoptosis · Antimetastasis · DNA fragmentation

✉ Pengcheng Li
Pengchengli89@outlook.com

¹ Department of the Oral and Maxillofacial Surgery, the First Affiliated Hospital of Hainan Medical University, No.31, Longhua Road, Haikou 570100, China

² Department of Oral Anatomy and Physiology, the First Affiliated Hospital of Harbin Medical University, Harbin 150001, China

Introduction

The majority (95%) of all cases of oral malignancy are caused by oral squamous cell carcinoma (OSCC), a kind of head and neck cancer. High rates of recurrence, aggressive local invasion, and cervical lymph node metastases are all hallmarks of this disease. Patients with OSCC still face an adverse prognosis despite significant advancements in its comprehensive therapies, such as radiotherapy, surgery, and chemotherapy [1]. Despite advances in treatment, the 5-year survival rate for this disease remains dismal at around 50–60% [2–5]. Therefore, understanding the OSCC migration and invasion process is crucial for creating compelling, tailored therapeutics and better patient prognostic results. Successful medical applications have been discovered for vincristine, paclitaxel, and homoharringtonine, and approximately a hundred other compounds are currently undergoing testing in humans. Due to the multidirectional action of flavonoids, they are chemicals that can play a substantial role in anticancer therapy [6–8]. Flavonoids, particularly flavones, have been proven *in vivo* and *in vitro* activity against tongue squamous carcinoma within a specific range of selectivity. Cell cycle progression was inhibited in the G0/G1 phase by apigenin, baicalein, and naringenin [9]. The development of tumor cells is suppressed, and apoptosis is triggered by flavone-3-ol derivatives such as epigallocatechin (EGC), epicatechin gallate (ECG), and epigallocatechin gallate (EGCG) [10].

In Traditional Chinese Medicine, ginseng is revered as the “King of Herbs” for its ability to boost energy levels, fortify the immune system, and drive away negative influences [11–13]. Ginsenosides, ginseng’s primary active component, are responsible for many of the herb’s pharmacological benefits. Recent research has proven total ginsenosides to have a potent anti-gastric cancer effect [14]. In contrast, ginsenoside Rb1, one of the most prominent prototype components of total ginsenosides, appears to have anti-gastric cancer potential due to its function in preventing stomach precancerous lesions. Ginsenoside Rb1 is a vital byproduct of gut microbiota [15]. Studies have shown that Rb1’s microbially converted metabolites have better therapeutic effects than Rb1, both *in vivo* and *in vitro*. Ginsenoside CK, for instance, exhibits more anticancer activity than ginsenoside Rb1 in breast and colon cancer *in vitro* models. Research on whether ginsenoside CK is more effective than ginsenoside Rb1 in combating gastric cancer is required. The mechanism by which ginsenoside Rb1 and CK fight cancer [16]. However, the identification of anti-cancer drugs is hampered by the complexity of stomach cancer’s pathophysiology, which involves various routes and targets. Network pharmacology is a systematic and all-encompassing field that makes it simple to obtain essential targets for drug therapy of diseases and to choose significant signaling targets for mechanism study. Considering these findings, using network pharmacology to investigate how ginsenoside Rb1 and CK work to prevent stomach cancer is an exciting new direction for the field. Ginsenosides, a class of triterpenoid saponins isolated from ginseng (*Panax ginseng* Meyer), have pharmacological effects due to their steroidal structure and are involved in inflammatory responses, activation of nerve growth factors, neuroprotective processes, the cardiovascular system, angiogenesis, and the regulation of glucose and insulin metabolism [17–19]. In addition to their anticancer property, ginsenosides disrupt cancer cell growth by hastening apoptosis, cell cycle arrest, and autophagy. Among 150 forms of ginsenosides, Rb1 and Rg1 are the most numerous and responsible for the pharmacological effects of ginseng [20]. The anticancer impact of DNA-damaging drugs in hepatoblastoma has been demonstrated to be enhanced by

ginsenoside Rg1, which also stimulates the migration and proliferation of epithelial progenitor and neural stem cells [21]. Despite prior reports of the anticancer effects of ginsenosides Rg3 and Rg5, the impact of ginsenoside Rg1 on cancer remains unclear.

Despite the lack of clarity on the underlying mechanisms, many studies have revealed that ginsenoside Rg1 (GRb1) has a favorable or unfavorable influence on cell proliferation in various cell types. To give experimental data for further study and clinical practice, we plan to explore the function of GRb1 at different concentrations and in different cells in apoptosis investigations. Our preliminary findings stimulate further inquiry, encouraging the potential application of GRb1 in combatting human oral squamous cancer cells.

Materials and Methods

Materials and Reagents

Ginsenoside Rb1 (GRb1) was obtained from Nanjing DASF Biotechnology Co., Ltd. (Nanjing, China). RPMI-1640 medium, phosphate-buffered saline (PBS) was bought from Hyclone (Logan, UT, USA). CCK-8 was purchased from J&K Scientific Ltd. (Beijing, China). Crystal Violet was acquired from Aladdin Bio-Chem Technology Co., Ltd. (Shanghai, China). AO-EB and Hoechst 33342 were purchased from Huafeng United Technology Co., Ltd. (Beijing, China). Annexin V-fluorescein isothiocyanate (FITC)/propidium iodide (PI) apoptosis detection kit was ordered from Thermo Fisher Scientific (Shanghai, China). Fetal bovine serum (FBS), penicillin/streptomycin and trypsin were purchased from Gibco BRL (Gaithersburg, MD, USA). All the antibodies were purchased from Beyotime Co., Ltd. (Shanghai, China). Milli-Q (Millipore) deionized (DI) water (18.2 M Ω cm) was used during the whole experiment.

To confirm apoptotic cells, they were analyzed using a FACSCantoII flow cytometer (BD Bioscience, Heidelberg, Germany). The color intensity of the DMSO solution was measured at 490 nm using a microplate spectrophotometer (SpectroAmaxTM 250). IC₂₅ and IC₅₀ values (concentration of sample causing 50% loss of cell proliferation of the vehicle color control) were calculated using non-linear regression curve fitting of the dose-color control response plots on GraphPad Prism V.8.0 software. Fluorescence microscopy OLYMPUS CKX53 was used for fluorescence imaging.

Cell Culture and Maintenance and Cell Counting Kit-8 (CCK-8) Assay

Human oral squamous cancer cells (PCI-9A and PCI-13) were acquired from the Shanghai Institutes for Biological Sciences, Chinese Academy of Sciences. These cell lines were cultured in RPMI-1640 with 10% fetal bovine serum (FBS) under humidified conditions of 37 °C and 5% CO₂.

Cell Counting Kit-8 (CCK-8) provides an appropriate and robust way of achieving a cell viability assay. The PCI-9A and PCI-13 cell line was seeded at a density of 3×10^3 per well in a 96-well plate. The cells were then exposed to GRb1. Next, 10 μ L of CCK-8 was added to each well at 24 h. After 4 h of incubation, the absorbance of each well at 455 nm was assessed on a microplate reader [22].

Colony Formation Assay

Colony formation assay is an in vitro cell survival assay based on the capability of a single cell to spread into a colony [23]. The PCI-9A and PCI-13 cell line was seeded at a density of 3×10^3 per well in a 6-well plate. The cells were exposed to GRb1 (IC₂₅ and IC₅₀ concentration) for 24 h. After culturing, the cells were placed in ethanol for 30 min and then dyed with crystal violet (0.5%) for 10 h. After gently soaking with PBS thrice, we obtained colony images and totaled the established colonies.

Live Cell Staining

Live cell nuclear stains are used for cell tracking or as counterstains with fluorescent dyes or cells. The PCI-9A and PCI-13 cells (3×10^3 cells per well) were planted in 6-well plates for 24 h. They were then exposed to GRb1 (IC₂₅ and IC₅₀ concentration) for 24 h. Next, the cells were stained with AO-EB according to the manufacturer's guidelines. Images were obtained using an Olympus CKX53 microscope [24].

Nuclear Damage Staining

The PCI-9A and PCI-13 cells (3×10^3 cells per well) were planted in 6-well plates for 24 h. They were then exposed to GRb1 (IC₂₅ and IC₅₀ concentration) for 24 h. Subsequently, the cells were stained with Hoechst 33342 according to the manufacturer's guidelines. Images were obtained using an Olympus CKX53 microscope [25].

Apoptosis Analysis

The PCI-9A and PCI-13 cells (3×10^3 cells per well) were planted in 6-well plates for 24 h. The cells were then exposed to GRb1 (IC₂₅ and IC₅₀ concentration) for 24 h. Next, the cells were collected and dyed with Annexin V-FITC and PI. Flow cytometry instruments were used to investigate these apoptotic cells [26].

Analysis of Mitochondrial Membrane Potential (MMP)

The PCI-9A and PCI-13 cells (3×10^3 cells per well) were planted in 6-well plates for 24 h. The cells were then exposed to GRb1 (IC₂₅ and IC₅₀ concentration) for 24 h. Then, the cells were dyed with Rhodamine-123 (Rh-123) according to the manufacturer's guidelines and subsequently imaged using an Olympus CKX53 microscope.

Measurement of Reactive Oxygen Species (ROS) Superoxide Dismutase (SOD) and Catalase (CAT) Activity Assay

The accumulation of intracellular ROS was assessed using 2',7'-dichlorofluorescein diacetate (H2DCF-DA). The PCI-9A and PCI-13 cells (3×10^3 cells per well) were seeded in 6-well plates for 24 h and exposed to GRb1 (IC₂₅ and IC₅₀ concentration)

for 24 h. Then, the cells were stained with H₂DCF-DA according to the manufacturer's guidelines. Images were obtained using an Olympus CKX53 microscope.

The SOD and CAT biochemical assays were accomplished to examine the endogenous antioxidant activity in GRb1 (IC₂₅ and IC₅₀ concentration) for 24 h. In brief, after incubation of PCI-9A and PCI-13 cells, homogenizations, and centrifugations, the Bradford assay evaluated the protein contents in the supernatant solutions. Later, a pre-determined ratio of proteins was employed for the enzyme assay [27].

Wound Healing Assay

The PCI-9A and PCI-13 cells were planted in 6-well plates at the density of 3×10^3 cells per well. The cells were then scratched and photographed for 0 h before GRb1 (IC₂₅ and IC₅₀ concentration) treatment for 24 h (IC₂₅ and IC₅₀ concentration). For more details, please refer to the previous study. The cells were imaged using an Olympus CKX53 microscope [28].

Transwell Assays

Transwell assays were accomplished using 24-well transwell permeable supports with Matrigel coating. The PCI-9A and PCI-13 cells (3×10^3) were seeded into the top transwell chamber, a 48-well plate with 200 μ L of serum media (1%). After that, 800 μ L of a 10% serum culture medium for cells was added to the lower well. The top chamber was removed from the culture vessel and washed twice after 24 h of incubation. The top layer of the container was then cleaned with a damp cotton swab without disrupting the cells underneath. The cells were visualized after being stained for 12 h with 0.1% crystal violet and fixed in methanol for 30 min after cleaning the chamber thrice with phosphate-buffered saline. The cells were imaged using an Olympus CKX53 microscope [29].

Statistical Analysis

Statistical analyses were examined with GraphPad Prism 8.0. The outcomes were displayed as mean \pm standard deviation values. The Student's *t*-tests were used for differences between all groups. P-values < 0.05 were believed to be statistically significant. All triplicate results were quantifications of independent tests.

Results and Discussion

Cell Proliferation on PCI-9A and PCI-13 Cells

To investigate the cell viability of GRb1, cells were treated with different doses of GRb1 for 24 h (Fig. 1A and B). The effect of GRb1 on cell proliferation was dose-dependently reduced in PCI-9A and PCI-13 cell lines. The IC₂₅ and IC₅₀ values of GRb1 in PCI-9A and PCI-13 cells were 64 μ g/mL and 56 μ g/mL, respectively. The bright field images of cancerous PCI-9A and PCI-13 cells are displayed in Fig. 1C. The results indicate cell proliferation in the PCI-9A and PCI-13 cells enhanced this proliferation after the treatment. This is strong evidence of the GRb1 treated with IC₅₀

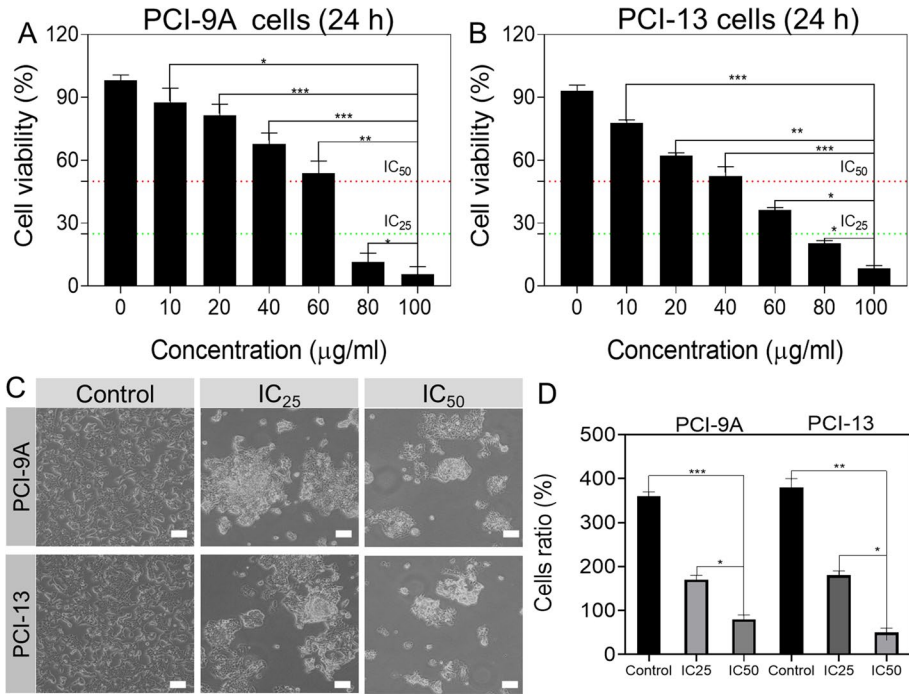


Fig. 1 PCI-9A and PCI-13 cells were incubated with GRb1 (10, 20, 40, 60, 80, 100 µg/mL) for 24 h (**A** and **B**) and cell viability was detected by CCK-8. **C** The bright field cell morphology images represent the PCI-9A and PCI-13 cells. **D** The cell ratio of IC₂₅ and IC₅₀ concentrations of GRb1 in PCI-9A and PCI-13 for 24 and 48 h. Scale bar = 100 µm. Error bars represent mean ± SD, **P* < 0.05, ***P* < 0.01, and ****P* < 0.001 (*n* = 6)

concentration selectively killing cancer cells (Fig. 1D). While most studies highlight cytotoxicity, it is vital to note GRb1 impacts on cellular behaviors. The tendency of many malignant tumors to metastasize is the primary cause of cancer fatalities. Tumor cell migration is recognized as an essential phase in cancer development and metastasis. Consistent with previous findings, we found that GRb1 significantly inhibited the migration and invasion of papillary thyroid carcinoma cells, suggesting a possible role for GRb1 in the metastasis of papillary thyroid cancer. Furthermore, GRb1 has been shown in previous studies to increase nuclear fragmentation and condensation, inhibiting the migration and invasion of ovarian cancer cells. GRb1 has also been shown to limit the migration of pancreatic cancer cells by affecting bidirectional interaction with pancreatic stellate cells.

Additionally, we performed a colony formation assay to demonstrate the effect of treatment with GRb1. The PCI-9A and PCI-13 cells were incubated with IC₂₅ and IC₅₀ concentrations of 24 h. As shown in Fig. 2A and B, PCI-9A and PCI-13 cells treated at IC₂₅ and IC₅₀ concentrations significantly affected the colony formation for the control cells. However, the GRb1 treatment significantly inhibited these colony formations. These findings suggested that PCI-9A and PCI-13 cells with GRb1 with IC₅₀ concentration synergistically reduced cell viability against PCI-9A and PCI-13 oral squamous cancer cells.

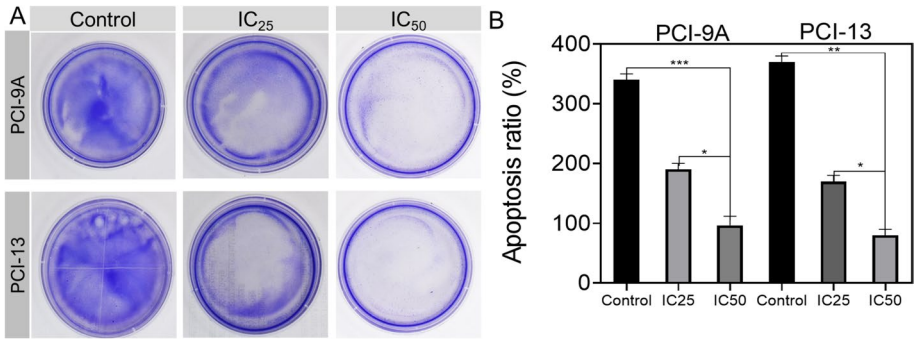


Fig. 2 Colonogenic assay. **A** Representative images. **B** Colony forming efficiency from clonogenic survival assays indicate that pretreatment of PCI-9A and PCI-13 cells was incubated with IC₂₅ and IC₅₀ concentrations of GRb1 for 24 h. Error bars represent mean ± SD, **P* < 0.05, ***P* < 0.01, and ****P* < 0.001 (*n* = 6)

Morphological Changes in PCI-9A and PCI-13 Cells

Bright-field microscopical images were employed to examine the cellular morphology in the PCI-9A and PCI-13 cells treated with the GRb1. These images revealed that at IC₂₅ and IC₅₀ concentrations, GRb1 reduced cell proliferation (Fig. 3A and B). Additionally, the morphological changes and apoptosis of GRb1-treated PCI-9A and PCI-13 cells at the IC₂₅ and IC₅₀ concentrations were analyzed using acridine orange and ethidium bromide. Cells with apoptotic bodies and blebs in their membranes were observed. Ethidium bromide can only stain dead cells because it cannot traverse an intact plasma membrane. However, acridine orange can stain all types of control cells. This analysis showed no substantial cell death in the untreated or control cells (Fig. 3A). The study showed that with the IC₂₅ and IC₅₀ concentrations of GRb1, there was an improvement in apoptotic cells compared with IC₂₅ concentration. The broken cells had significant morphological changes, suggesting that IC₅₀ concentrations of GRb1 induce apoptosis and are highly cytotoxic to the PCI-9A and PCI-13 oral squamous cancer cell line. These results confirmed that IC₅₀

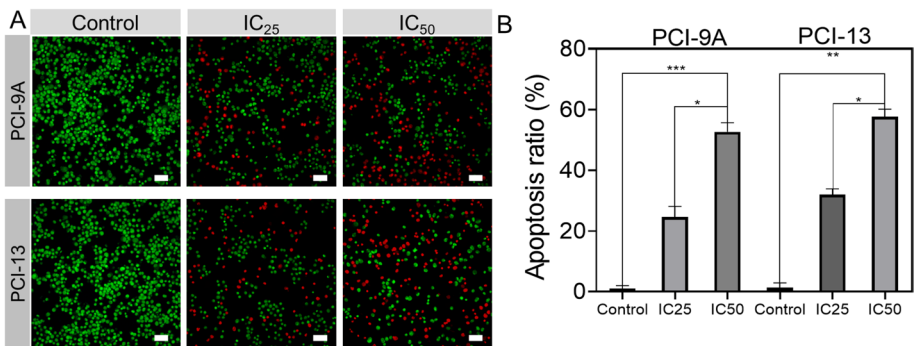


Fig. 3 Morphological observation of PCI-9A and PCI-13 cells was incubated with IC₂₅ and IC₅₀ concentrations of GRb1 for 24 h. **A** Acridine orange-ethidium bromide (AO-EB) staining. Scale bar = 100 μm. **B** Respective apoptosis ratio. Error bars represent mean ± SD, **P* < 0.05, ***P* < 0.01, and ****P* < 0.001 (*n* = 6)

concentrations of GRb1 played a crucial role in the apoptosis of both cancer cells, which correlated with the results of previous studies.

Hoechst 33342, often known as nucleic acid blue, is a cell-permeable fluorescent dye. As it stains the fragmented nuclei of apoptotic cells, it enhances the observation of chromatin condensation and fragmentation. The apoptotic impact of GRb1 in PCI-9A and PCI-13 cells was examined using this dye. There were significantly more apoptotic bodies in the IC₂₅ and IC₅₀ treatment groups compared to the control group (Fig. 4A and B). The healthy control cells were oval. In contrast, cells treated with IC₂₅ and IC₅₀ concentrations of GRb1 displayed apoptosis characteristics such as cell shrinkage, extremely fragmented and condensed nuclei, generation of several apoptotic bodies, and cell fragmentation and decrement. It has been hypothesized that apoptosis is the primary mechanism of cell death caused by the cytotoxic impact of IC₅₀ concentrations of GRb1. Our results demonstrated that apoptosis was induced in PCI-9A and PCI-13 oral squamous cancer cells when exposed to IC₅₀ concentrations of GRb1.

Annexin V-FITC Assay

Flow cytometric analysis using Annexin V-FITC/propidium iodide double-staining was used to gain an understanding of the apoptotic impact generated by GRb1. Since Annexin V-FITC has a high affinity for phosphatidylserine, which is responsible for transporting Annexin V-FITC from the inner leaflet of the plasma membrane's leaflet to the outer surface of the membrane during early apoptosis, the presence of these two stains indicated cells were in early apoptosis. Propidium iodide, which cannot pass via an intact cell membrane, penetrates the damaged membranes of dead or late apoptotic cells and binds to nucleic acids, identifying necrotic cells as Annexin V-FITC. Annexin V-FITC and propidium iodide negative cells are alive, whereas Annexin V-FITC and propidium iodide positive cells are in the late stages of apoptosis. Increasing percentages of treated cells in early and late apoptosis were seen in the example dot plots for the flow cytometric study comparing untreated cells with treated cells (24 h) (Fig. 5A and B). In addition, exposure increases the number of dead cells at 24 h. These results suggest that the antiproliferative effect of IC₅₀ concentrations of GRb1 on PCI-9A and PCI-13 cells results from the

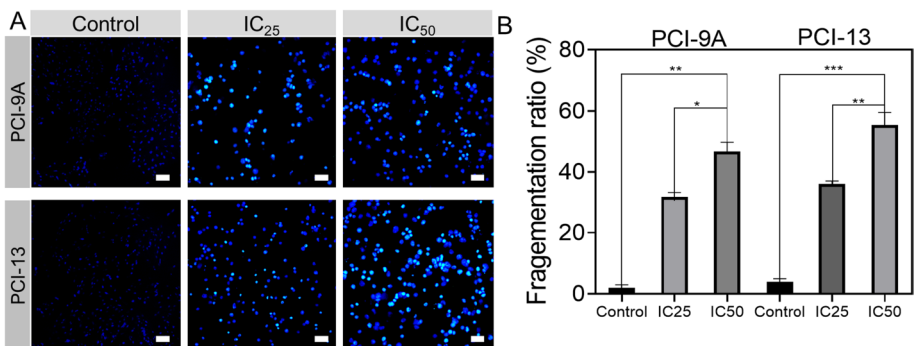


Fig. 4 Nuclear fragmentation of PCI-9A and PCI-13 cells was incubated IC₂₅ and IC₅₀ concentrations of GRb1 for 24 h. **A** The changes were observed with DAPI nuclear staining of the treated cells. Scale bar = 100 μ m. **B** Respective fragmentation ratio. Error bars represent mean \pm SD, * P < 0.05, ** P < 0.01, and *** P < 0.001 (n = 6)

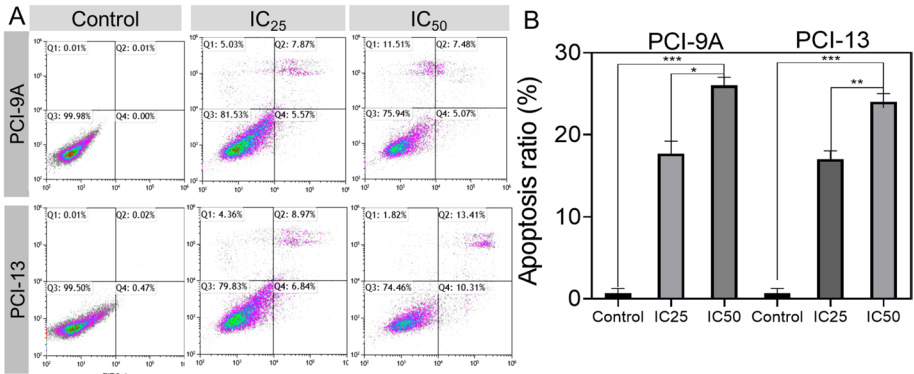


Fig. 5 Apoptosis induced by PCI-9A and PCI-13 cells were incubated with IC₂₅ and IC₅₀ concentrations of GRb1 for 24 h. **A** Cells were stained with Annexin V-FITC and PI. Flow cytometry analyzed apoptosis in 4T1 cancer cells. **B** Respective apoptosis ratio. Error bars represent mean \pm SD, * $P < 0.05$, ** $P < 0.01$, and *** $P < 0.001$ ($n = 6$)

induction of cell apoptosis. The results were compared with GRb1 with other cancer cells and nanoparticles.

Apoptosis Signaling Pathway

Apoptosis is triggered by many signaling pathways when mitochondrial membrane integrity is compromised due to excess ROS. The rhodamine 123 (Rho123) staining experiment was employed to see how nanomaterials affected mitochondrial membrane potential (Fig. 6A and B). Compared to control PCI-9A and PCI-13 cells, the fluorescent signal reduction caused by treatment with GRb1 depolarized the MMP. This depolarization and high ROS in the mitochondria resulted in the outer membrane rupture. They enlarged the mitochondrial matrix and have both been described as essential features in apoptosis

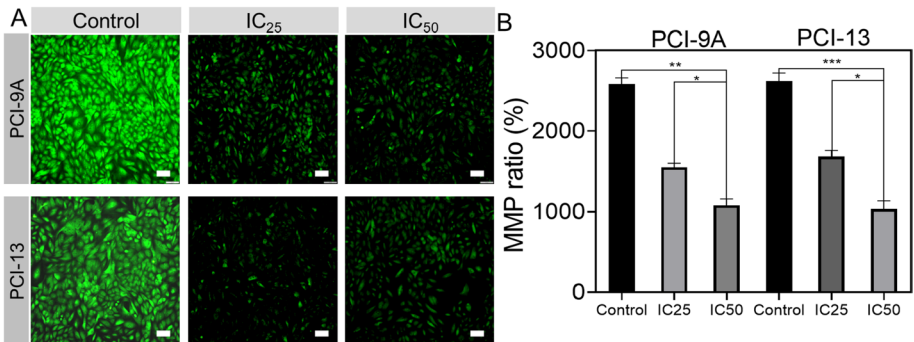


Fig. 6 Rhodamine 123 staining of PCI-9A and PCI-13 cells. Rhodamine 123 assay images. **A** Mitochondrial membrane potential assay by IC₂₅ and IC₅₀ concentrations of GRb1 for 24 h. Scale bar = 100 μ m. **B** Quantification of Fluorescence intensity of MMP. Error bars represent mean \pm SD, * $P < 0.05$, ** $P < 0.01$, and *** $P < 0.001$ ($n = 6$)

(Fig. 6B). Thus, the IC_{25} and IC_{50} concentrations of GRb1 cause the MMP to depolarize, enhancing the outer membrane's permeability and activating several other molecular components.

Using a fluorogenic probe (DCFH-DA), we detected ROS generation by GRb1 in real time. This probe quickly permeates cell membranes due to its minor, nonpolar nature. It undergoes deacetylation by esterases upon intracellular entry, transforming into a polar, non-fluorescing molecule. The high levels of ROS within cells can oxidize it to 2,7-dichlorofluorescein (DCF), a highly luminous green fluorescent dye. The findings demonstrate an increased ROS production, with GRb1 displaying an IC_{25} and IC_{50} concentration (Fig. 7A and B). GRb1 functions as a redox system in cancer cells, reacting with cellular components to produce significant ROS levels, contributing to oxidative stress (Fig. 7C and D). This, in turn, leads to membrane damage by lipid peroxidation and protein denaturation, culminating in necrosis and DNA damage, ultimately triggering cell death via apoptosis. Enzyme action assessment suggested the reduced ratio of SOD and CAT action after incubating PCI-9A and PCI-13 cells with GRb1 (IC_{25} and IC_{50} concentrations) for 24 h. This data showed that IC_{25} and IC_{50} concentrations of GRb1 may promote apoptosis and oxidative stress by deactivating CAT (Fig. 7C) and SOD (Fig. 7D) in the PCI-9A and PCI-13 cells. To further investigate the impact of IC_{25} and IC_{50} concentrations of GRb1 facilitated by ROS on the generation of cell death, the PCI-9A and PCI-13 cells were co-incubated with the IC_{25} and IC_{50} concentrations of IC_{25} and IC_{50} concentrations of GRb1 (Fig. 7C and D). Co-incubation showed reduced ROS generation and apoptosis, potentially due to the antioxidant properties of IC_{25} and IC_{50} concentrations of GRb1. This further implies

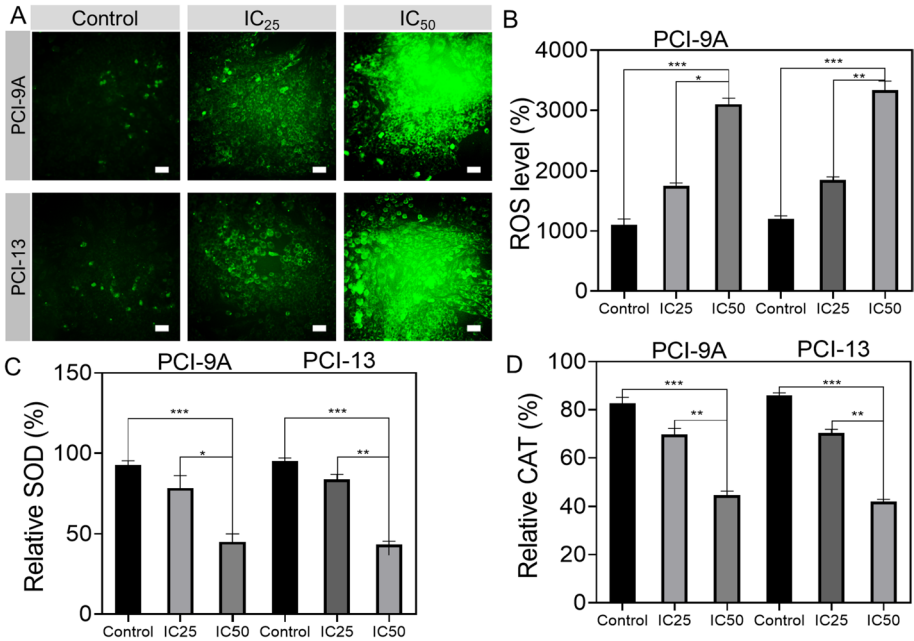


Fig. 7 A ROS generation assay images. ROS generation induced by IC_{25} and IC_{50} concentrations of GRb1 for 24 h in PCI-9A and PCI-13 cancer cells. Scale bar = 100 μ m. B Quantification of 2'-7' dichlorofluorescein (DCF) intensity. C Percentage of SOD activity after incubation with IC_{25} and IC_{50} concentrations of GRb1. D Percentage of CAT activity after incubation with IC_{25} and IC_{50} concentrations of GRb1

that GRb1 incubation triggers apoptosis by elevating intracellular ROS levels in PCI-9A and PCI-13 cells.

DNA Fragmentation Assay

GRb1-induced toxicity was associated with oxidative stress. Treating cells with GRb1 can lead to GSH depletion, induce oxidative stress, and increase ROS production. Reactive oxygen species (ROS) can cause genotoxic damage, cell malfunction, and cell death by attacking biomolecules. GRb1 has been shown to cause apoptosis in normal tissues in several *in vitro* and *in vivo* experiments. In addition, investigations have shown GRb1 to be genotoxic via testing for chromosome aberrations, micronucleus formation, and comet formation. These experiments confirm our findings and reveal that GRb1 significantly increased DNA fragmentation. The alkaline comet assay was employed to identify DNA breaks in the PCI-9A and PCI-13 cells for 24 h treatment with the GRb1 in IC₂₅ and IC₅₀ concentrations (Fig. 8A and B). Compared to the control cells (showing minimal DNA fragmentation), IC₂₅ and IC₅₀ concentrations of GRb1 displayed improved DNA breaks at the IC₂₅ and IC₅₀ concentrations. This contrasted with the GRb1, where only marginal activity was evident, demonstrating a high ratio of tail formation in IC₅₀ concentrations of GRb1 compared to IC₂₅ concentration (Fig. 8B).

In Vitro Migration and Invasion Assay

ECM plays a crucial role in preventing metastasis, which is a complicated process in and of itself. Cell invasion is identical to cell migration in an *in vitro* migration and invasion experiment, except that invading cells must break down and travel through an extracellular matrix (ECM) barrier. Both migratory and invasion experiments yielded statistically significant findings (Fig. 9A and B). To quantify the inhibitory impact of different formulations on PCI-9A and PCI-13 migration, wound healing, transwell cell migration, and invasion tests were conducted based on the previous investigation's overall outcomes, including CCK-8 analysis, apoptosis staining methods, DNA fragmentation assay, and mitochondrial membrane potential assays, GRb1 exhibited remarkable cytotoxicity in PCI-9A and PCI-13

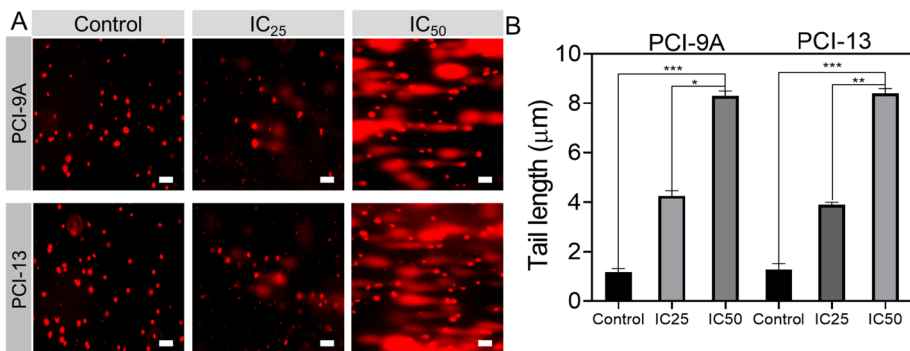


Fig. 8 Comet assay images. **A** DNA fragmentation induced by IC₂₅ and IC₅₀ concentrations of GRb1 for 24 h in PCI-9A and PCI-13 cancer cells. Scale bar = 200 µm. **B** Respective tail length ratio. Error bars represent mean ± SD, **P* < 0.05, ***P* < 0.01, and ****P* < 0.001 (*n* = 6)

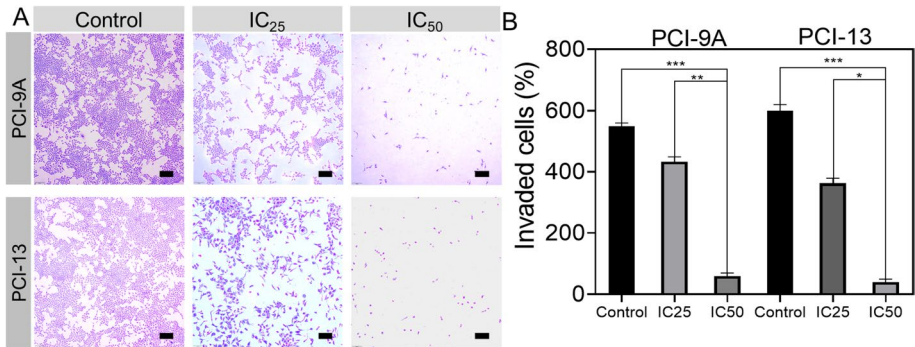


Fig. 9 In vitro inhibitory effects of IC₂₅ and IC₅₀ concentrations of GRb1 for 24 h in PCI-9A and PCI-13 on cell invasion. **A** Transwell invasion assay. Scale bar = 100 μ m. **B** Respective invaded cells ratio. Error bars represent mean \pm SD, * P < 0.05, ** P < 0.01, and *** P < 0.001 (n = 6)

cells. The in vitro migration assay was performed at pH 7.4. In the wound healing experiment, the scratched gap was scarcely visible in the control group 24 h after incubation (Fig. 10A and B). The wound closure rates in the IC₂₅ and IC₅₀ concentrations of GRb1 groups were 75.2% and 60.9%, respectively. The percentage of time taken for wounds to heal decreased from the control group (44.5%) to the IC₂₅ and IC₅₀ concentrations of the GRb1-treated group (15.9%) (Fig. 11A and B). Based on this data, PCI-9A and PCI-13 cells exhibited significant motility, with IC₅₀ concentrations of GRb1 proving the most effective for suppressing cell movement. The number of migrated cells was lower in the IC₂₅ concentrations of GRb1-treated groups compared to the control in the Transwell migration experiment. In the GRb1 cohort, the number dropped even further. However, in the GRb1 with IC₅₀ concentrations of the GRb1 group, the number of migrating cells drastically decreased in both PCI-9A and PCI-13 cancer cells (Fig. 10A). The invasion experiment (Fig. 9A) confirmed the inhibitory impact of IC₅₀ concentrations of the GRb1. Notably, the most significant inhibition of PCI-9A and PCI-13 cell migration and invasion was observed with IC₅₀ concentrations of the GRb1, suggesting that this may have enhanced anti-metastasis effectiveness in vivo.

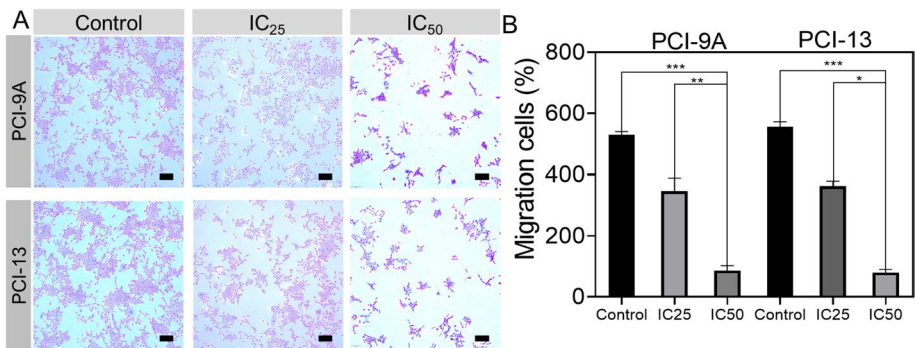


Fig. 10 In vitro inhibitory effects of PCI-9A and PCI-13 cells were incubated with IC₂₅ and IC₅₀ concentrations of GRb1 for 24 h on cell migration. **A** Transwell migration assay. Scale bar = 100 μ m. **B** Respective migration cells ratio. Error bars represent mean \pm SD, ** P < 0.01 and *** P < 0.001 (n = 6)

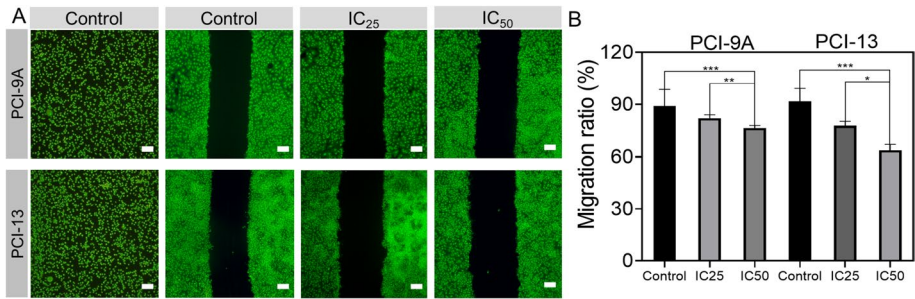


Fig. 11 In vitro inhibitory effects of PCI-9A and PCI-13 cells were incubated with IC₂₅ and IC₅₀ concentrations of GRb1 for 24 h on cell scratch wound-healing. **A** Typical images of scratch wound-healing assays. Scale bar = 40 μ m. **B** Respective migration cells ratio. Error bars represent mean \pm SD, ** $P < 0.01$ and *** $P < 0.001$ ($n = 6$)

Conclusion

In conclusion, this analysis explored Ginsenoside Rb1 (GRb1) for oral squamous cancer treatment. In vitro, cytotoxicity studies confirmed that GRb1 was more effective in PCI-9A and PCI-13 cells. The different biochemical staining methods confirmed the morphological investigation of the cells. In addition, the antimetastatic properties of GRb1 were investigated by the tube formation assay and Transwell migration assay, which revealed excellent metastatic properties. The DNA fragmentation of the PCI-9A and PCI-13 cells was assessed using a comet assay. GRb1 improved ROS levels and caused mitochondrial membrane potential and DNA damage, which resulted in apoptosis. Therefore, this study suggests the potential of GRb1 for oral squamous cancer therapy. Considering its favorable advantages of GRb1 as per the previous reports and present reports, GRb1 holds promise as a viable intelligent drug delivery approach, with substantial potential for preclinical translation in various cancer cells, including oral squamous cancer therapy, subject to validation using in vivo animal models in the future.

Author Contribution Le An, and Yang Yu: conceptualization, writing, data curation, software, writing original draft, methodology. Long He: analyzed and interpreted the data, resources, contributed reagents. Xu Xiao: materials, analysis data, software. Pengcheng Li: conceptualization, project administration, writing—review and editing

Data Availability All data generated or analyzed during this research are included in this published article.

Declarations

Conflict of Interest No potential conflict of interest was reported by the authors.

Ethics Approval NA.

Consent to Participate NA.

Consent for Publication All authors agreed to publish this paper in this journal.

References

1. de Mendoza, I. L. I., Mendia, X. M., de la Fuente, A. M. G., Andres, G. Q., & Urizar, J. M. A. (2020). Role of *Porphyromonas gingivalis* in oral squamous cell carcinoma development: A systematic review. *Journal of Periodontal Research*, *55*, 13–22.
2. Das, N., Hussain, E., & Mahanta, L. B. (2020). Automated classification of cells into multiple classes in epithelial tissue of oral squamous cell carcinoma using transfer learning and convolutional neural network. *Neural Networks*, *128*, 47–60.
3. Liu, L., Chen, J., Cai, X., Yao, Z., & Huang, J. (2019). Progress in targeted therapeutic drugs for oral squamous cell carcinoma. *Surgical Oncology*, *31*, 90–97.
4. Cristaldi, M., Mauceri, R., Di Fede, O., Giuliana, G., Campisi, G., & Panzarella, V. (2019). Salivary biomarkers for oral squamous cell carcinoma diagnosis and follow-up: Current status and perspectives. *Frontiers in Physiology*, *10*, 1476.
5. Jiang, X., Wu, J., Wang, J., & Huang, R. (2019). Tobacco and oral squamous cell carcinoma: A review of carcinogenic pathways. *Tobacco Induced Diseases*, *17*.
6. Capote-Moreno, A., Brabyn, P., Muñoz-Guerra, M. F., Sastre-Pérez, J., Escorial-Hernandez, V., Rodríguez-Campo, F. J., García, T., & Naval-Gías, L. (2020). Oral squamous cell carcinoma: Epidemiological study and risk factor assessment based on a 39-year series. *International Journal of Oral and Maxillofacial Surgery*, *49*, 1525–1534.
7. Alabi, R. O., Youssef, O., Pirinen, M., Elmusrati, M., Mäkitie, A. A., Leivo, I., & Almagush, A. (2021). Machine learning in oral squamous cell carcinoma: Current status, clinical concerns and prospects for future—A systematic review. *Artificial Intelligence in Medicine*, *115*, 102060.
8. Ling, Z., Cheng, B., & Tao, X. (2021). Epithelial-to-mesenchymal transition in oral squamous cell carcinoma: challenges and opportunities. *International Journal of Cancer*, *148*, 1548–1561.
9. Bugshan, A., & Farooq, I. (2020). Oral squamous cell carcinoma: metastasis, potentially associated malignant disorders, etiology and recent advancements in diagnosis. *F1000Research*, *9*.
10. Almagush, A., Mäkitie, A. A., Triantafyllou, A., de Bree, R., Strojan, P., Rinaldo, A., Hernandez-Prera, J. C., Suárez, C., Kowalski, L. P., & Ferlito, A. (2020). Staging and grading of oral squamous cell carcinoma: An update. *Oral Oncology*, *107*, 104799.
11. Li, H., & Li, H. (2020). Ginsenoside-Rg5 inhibits growth and metastasis of ovarian carcinoma via suppressing expression of fibroblast growth factor-8b (FGF8b). *Journal of King Saud University-Science*, *32*, 1162–1167.
12. Shan, K., Wang, Y., Hua, H., Qin, S., Yang, A., & Shao, J. (2019). Ginsenoside Rg3 combined with oxaliplatin inhibits the proliferation and promotes apoptosis of hepatocellular carcinoma cells via downregulating PCNA and cyclin D1. *Biological and Pharmaceutical Bulletin*, *42*, 900–905.
13. Qu, L., Liu, Y., Deng, J., Ma, X., & Fan, D. (2023). Ginsenoside Rk3 is a novel PI3K/AKT-targeting therapeutics agent that regulates autophagy and apoptosis in hepatocellular carcinoma. *Journal of Pharmaceutical Analysis*, *13*, 463–482.
14. Hong, H., Baatar, D., & Hwang, S. G. (2021). Anticancer activities of ginsenosides, the main active components of ginseng. *Evidence-Based Complementary and Alternative Medicine*, *2021*.
15. Zhu, H., He, Y.-S., Ma, J., Zhou, J., Kong, M., Wu, C.-Y., Mao, Q., Lin, G., & Li, S.-L. (2021). The dual roles of ginsenosides in improving the anti-tumor efficiency of cyclophosphamide in mammary carcinoma mice. *Journal of Ethnopharmacology*, *265*, 113271.
16. Zhang, J., Ma, X., & Fan, D. (2021). Ginsenoside CK inhibits hypoxia-induced epithelial–mesenchymal transformation through the HIF-1 α /NF- κ B feedback pathway in hepatocellular carcinoma. *Foods*, *10*, 1195.
17. Zhu, H., Wang, S.-Y., Zhu, J.-H., Liu, H., Kong, M., Mao, Q., Zhang, W., & Li, S.-L. (2021). Efficacy and safety of transcatheter arterial chemoembolization combined with ginsenosides in hepatocellular carcinoma treatment. *Phytomedicine*, *91*, 153700.
18. Hwang, H. J., Hong, S. H., Moon, H. S., Yoon, Y. E., & Park, S. Y. (2022). Ginsenoside Rh2 sensitizes the anti-cancer effects of sunitinib by inducing cell cycle arrest in renal cell carcinoma. *Scientific Reports*, *12*, 19752.
19. Qu, L., Ma, X., & Fan, D. (2021). Ginsenoside Rk3 suppresses hepatocellular carcinoma development through targeting the gut-liver axis. *Journal of Agricultural and Food Chemistry*, *69*, 10121–10137.
20. Yang, X., Li, Y., & Qian, H. (2020). Study on the selection of the targets of esophageal carcinoma and interventions of ginsenosides based on network pharmacology and bioinformatics. *Evidence-Based Complementary and Alternative Medicine*, *2020*.
21. Ren, Z., Chen, X., Hong, L., Zhao, X., Cui, G., Li, A., Liu, Y., Zhou, L., Sun, R., Shen, S., Li, J., Lou, J., Zhou, H., Wang, J., Xu, G., Yu, Z., Song, Y., & Chen, X. (2020). Nanoparticle conjugation of

- ginsenoside Rg3 inhibits hepatocellular carcinoma development and metastasis. *Small*, *16*, 1905233. <https://doi.org/10.1002/smll.201905233>
22. Cai, L., Qin, X., Xu, Z., Song, Y., Jiang, H., Wu, Y., Ruan, H., & Chen, J. (2019). Comparison of cytotoxicity evaluation of anticancer drugs between real-time cell analysis and CCK-8 method. *ACS Omega*, *4*, 12036–12042. <https://doi.org/10.1021/acsomega.9b01142>
 23. Li, J., Hu, S., Zhang, Z., Qian, L., Xue, Q., & Qu, X. (2020). LASP2 is downregulated in human liver cancer and contributes to hepatoblastoma cell malignant phenotypes through MAPK/ERK pathway. *Biomedicine & Pharmacotherapy*, *127*, 110154. <https://doi.org/10.1016/j.biopha.2020.110154>
 24. Velmurugan, P., Shim, J., Bang, K.-S., & Oh, B.-T. (2016). Gold nanoparticles mediated coloring of fabrics and leather for antibacterial activity. *Journal of Photochemistry and Photobiology B: Biology*, *160*, 102–109. <https://doi.org/10.1016/j.jphotobiol.2016.03.051>
 25. Pan, W., Gong, S., Wang, J., Yu, L., Chen, Y., Li, N., & Tang, B. (2019). A nuclear-targeted titanium dioxide radiosensitizer for cell cycle regulation and enhanced radiotherapy. *Chemical Communications*, *55*, 8182–8185. <https://doi.org/10.1039/C9CC01651A>
 26. Rudrappa, M., Rudayni, H. A., Assiri, R. A., Bepari, A., Basavarajappa, D. S., Nagaraja, S. K., Chakraborty, B., Swamy, P. S., Agadi, S. N., Niazi, S. K., & Nayaka, S. (2022). Plumeria alba-mediated green synthesis of silver nanoparticles exhibits antimicrobial effect and anti-oncogenic activity against glioblastoma U118 MG cancer cell line. *Nanomaterials*, *12*. <https://doi.org/10.3390/nano12030493>
 27. Li, K. G., Chen, J. T., Bai, S. S., Wen, X., Song, S. Y., Yu, Q., Li, J., & Wang, Y. Q. (2009). Intracellular oxidative stress and cadmium ions release induce cytotoxicity of unmodified cadmium sulfide quantum dots. *Toxicology in Vitro*, *23*, 1007–1013. <https://doi.org/10.1016/j.tiv.2009.06.020>
 28. Han, Y., Jiang, Y., Li, Y., Wang, M., Fan, T., Liu, M., Ke, Q., Xu, H., & Yi, Z. (2019). An aligned porous electrospun fibrous scaffold with embedded asiatic acid for accelerating diabetic wound healing. *Journal of Materials Chemistry B*, *7*, 6125–6138. <https://doi.org/10.1039/C9TB01327J>
 29. Chen, Q., Jiao, D., Yan, L., Wu, Y., Hu, H., Song, J., Yan, J., Wu, L., Xu, L., & Shi, J. (2015). Comprehensive gene and microRNA expression profiling reveals miR-206 inhibits MET in lung cancer metastasis. *Molecular BioSystems*, *11*, 2290–2302. <https://doi.org/10.1039/C4MB00734D>

Publisher's Note Springer Nature remains neutral with regard to jurisdictional claims in published maps and institutional affiliations.

Springer Nature or its licensor (e.g. a society or other partner) holds exclusive rights to this article under a publishing agreement with the author(s) or other rightsholder(s); author self-archiving of the accepted manuscript version of this article is solely governed by the terms of such publishing agreement and applicable law.